Progress In Electromagnetics Research Letters, Vol. 30, 49–58, 2012

TERAHERTZ INTERFEROMETER FOR INTEGRATED GOUBAU-LINE WAVEGUIDES

S. Laurette, A. Treizebre, N. E. Bourzgui, and B. Bocquet*

Institute of Electronics Microelectronics and Nanotechnology (IEMN), UMR CNRS 8520, University of Lille 1, Villeneuve d'Ascq, France

Abstract—An integrated Terahertz Mach-Zehnder interferometer is presented in order to perform differential measurements in a chip. Both simulation and experiment are performed for validating the interferometer structure. Destructive interference peaks are observed, and destructive frequencies are predicted by a mathematical model with a good agreement. The structure is then used to characterize dielectric constant of materials. Simulation results enable to quantify the device sensitivity. An experimental validation is given with the characterization of a thermosensitive polymer (Cyclotene BCB) in the sub-THz frequency band. Perspectives to increase investigated frequencies are discussed.

1. INTRODUCTION

Between mm-waves and optics, research on the Terahertz spectrum (0.1 THz–30 THz) is currently in huge expansion [1]. It is now known that such waves can advantageously deal with biological material [2, 3]. For instance, DNA-hybridization, protein conformation or hydration can be probed in real-time and marker-free conditions by THz waves which excite liquid weak-bond like hydrogen ones [4]. In order to perform THz spectroscopy, the waves can either be air-propagated [5] or guided [6]. However, in the first case, the probe spatial-resolution is limited by diffraction whereas in the second one, sub-wavelength resolutions can be obtained. This near-field approach is enabled by THz waveguides development. For instance, THz waves can be driven in a plasmon-like mode by a single metallic wire [7]. When this waveguide is made of a single wire deposited on a substrate, it is called "Planar Goubau Line" (PGL) and can reach spatial field-confinement

Received 12 December 2011, Accepted 13 February 2012, Scheduled 21 February 2012
* Corresponding author: Bertrand Bocquet (Bertrand.Bocquet@univ-lille1.fr).

down to several micrometers [8]. Such a configuration has already been integrated in biochips [9] to characterize enzymatic reactions [10] or molecule hydration [11].

In order to increase sensitivity of these devices and bring original measurement configurations, advanced functions on Goubau lines have to be developed. Transitions between coplanar waveguides and PGL have been previously reported [12] and sub-wavelength scaled spiral-resonators have been proposed in PGL [13]. PGL power dividers are now available [14, 15]. Goubau line wave-guiding up to 800 GHz has already been experimentally demonstrated [16], showing that this technology is well suited for THz investigation.

A Mach-Zehnder interferometer based on PGL technology for THz frequencies is presented here. Interferometers, by probing signal phases, have already been used for "Lab on Chip" devices in the optical spectrum to detect proteins or DNA hybridization [17, 18]. It is, to the best of our knowledge, the first time that this concept is both experimentally realized and theoretically described in the case of integrated THz waveguides (a first proof of principle computation can be found in [19]).

2. PGL INTERFEROMETER PRINCIPLE AND DESIGN

In the Mach-Zehnder interferometer, an initial beam s_i is divided in two secondary beams, s_1 and s_2, which are recombined, after a given distance, to form the s signal. The complex signal s depends on the optical path difference δ between the two secondary beams as follows:

$$s = s_0 e^{jk\delta/2} \cos\left(\frac{k\delta}{2}\right) \tag{1}$$

where s_0 is a complex constant and $k = 2\pi f/c$ the wave vector. $c = 3.10^8$ m/s is the light speed constant in vacuum and f the signal frequency. For some frequencies $f_{d,\,m}$, the two recombined signals are in phase opposition and the s signal is minimal. Equation (1) gives :

$$f_{d,\,m} = \frac{c}{2\delta} + m\frac{c}{\delta} \tag{2}$$

where m is an integer.

The PGL interferometer structure is given in Figure 1. A divider/combiner is used to split/combine the THz wave [14]. The exciting signal is provided up to 325 GHz by a Vectorial Network Analyzer (VNA) dedicated to coplanar waveguides (CPW). As a consequence, a CPW/Goubau transition [12] has been used to propagate the Goubau mode. Used PGL are 500 nm-high and 5 µm-wide gold wires deposited on a 350 µm-thick borosilicate glass (Pyrex)

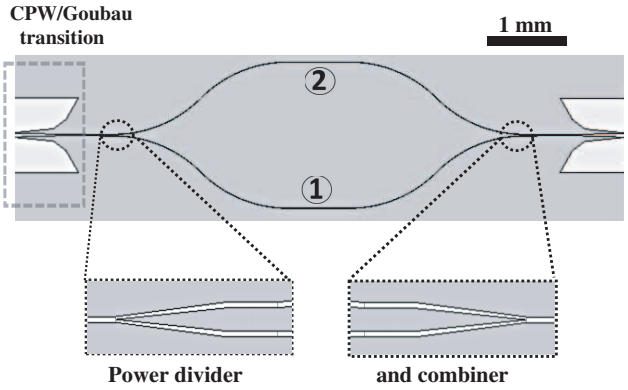

Figure 1. Interferometer design (equilibrated structure) with power divider and combiner excited through a coplanar/Goubau transition.

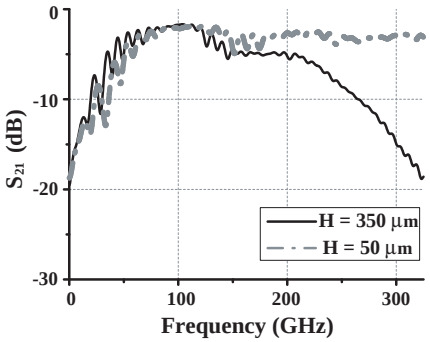

Figure 2. Transmission of the interferometer equilibrated-structure as a function of frequency and substrate thickness. Results from CST Microwave Studio simulations.

substrate. There is no simple mathematical model yet to describe wave propagation around them. However, since the propagation mode is a quasi-TEM one, the previously presented theory is expected to correctly predict the PGL interferometer behaviour.

Figure 2 shows the transmission S_{21} parameter of the equilibrated structure. There is no optical path difference between the two branches, consequently no destructive-interference frequency is observed. For the 350 µm-thick substrate ($H = 350\,\mu m$), a linear decrease of the transmitted signal is noticed for frequencies starting from 200 GHz. This shape is due to substrate-mode propagation in the pyrex substrate instead of Goubau-mode propagation. It can be reduced by decreasing the substrate thickness H, as shown in Figure 2 with $H = 50\,\mu m$. However, for the experimental validation, 350 µm-thick glass substrates

will be used. Thus, $H = 350\,\mu m$ will be systematically chosen for simulations in this study.

3. PGL INTERFEROMETER CHARACTERIZATION

3.1. Geometrical Path Difference

One way to create an optical path difference between the two recombined signals is to increase the wave geometrical-path of one of the two branches. If ΔL is the length difference between the two paths, thus $\delta = n\Delta L$, where n is the effective refractive index. With ε_g the glass substrate dielectric permittivity, this index can be evaluated by the empirical expression: $n = \sqrt{\frac{\varepsilon_g+1}{2}}$. Electromagnetic simulations have been performed with the CST Microwave Studio software to characterize the PGL interferometer non-equilibrated structures.

Figure 3(a) shows the non-equilibrated structure transmission parameter for two ΔL values. As expected, destructive interferences can be observed. The first destructive interference frequency $f_{d,0}$ is plotted as a function of ΔL for simulated structures in Figure 3(b) and is compared to the Equation (2) model with a good agreement. Thus, Equation (2) enables to quickly design an interferometer structure and to understand underlying phenomena.

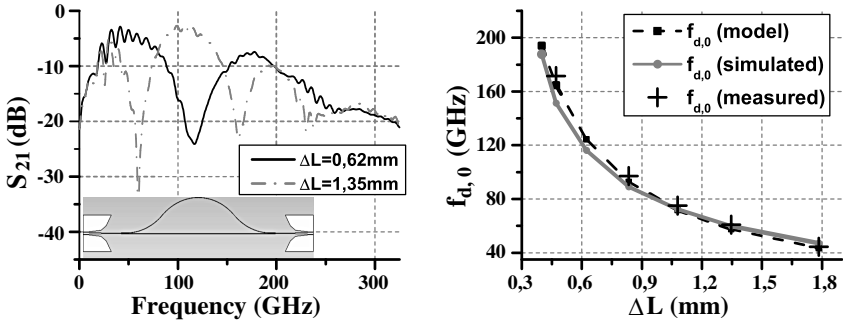

Figure 3. (a) Simulated transmission of the non-equilibrated structures as a function of frequency. (b) First destructive interference as a function of length difference between the two paths. For experimental measurements, crosses thickness corresponds to uncertainties.

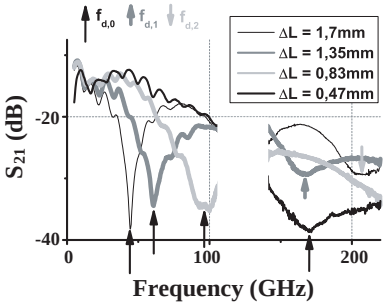

Figure 4. S_{21} measurement for several interferometer configurations. Vertical arrows indicate first, second and third destructive interference frequencies.

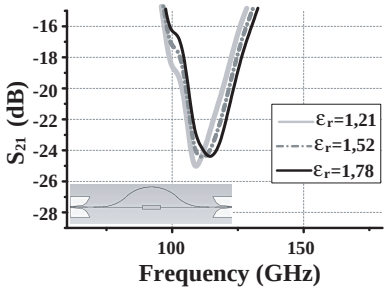

Figure 5. Influence of sample dielectric permittivity on interferometer transmission: First destruction interference shift.

3.1.1. Experimental Validation

Interferometers have been realized by a gold lift-off process on a 350 µm-thick glass substrate [9]. S_{21} parameter of the interferometers have been measured by an Agilent 8510XF VNA in the 0–110 GHz band and by a Rohde and Schwarz ZVA24 VNA in the 140–220 GHz band. Results are shown on Figure 4 and confirm simulation and model predictions in a very similar way.

First destructive interference frequencies $f_{d,0}$ are clearly shown. Second and third destructive frequencies $f_{d,1}$ and $f_{d,2}$ are indicated for two configurations. Experimental $f_{d,0}$ as a function of ΔL is reported in Figure 3(b) and is very close to simulated and modeled values. It can be noticed that increasing the destructive frequency value decreases the frequency measurement precision because peaks are broader. This can be explained by glass-loss increase with frequency which decreases interferometric fringes contrast. Using a low-loss quartz substrate should avoid the peak broadening with frequency.

3.2. Refractive Index Variations

In order to characterize the interferometer response to dielectric permittivity variations, the previous non-equilibrated structure has been used with $\Delta L = 0.62$ mm. As seen in Figure 5, a 100 µm-thick sample has been put on the first branch. Its permittivity is ε_r and its length is $l = 1$ mm. The electromagnetic field confinement around the PGL is about 10 µm for a 1 µm-wide PGL at 250 GHz [8]. Thus, in this simulation, the electromagnetic field is expected to be confined in

Table 1. Interferometer sensitivity for several non-equilibrated structure.

ΔL (mm)	1.34	0.83	0.62
f_0 (GHz)	59.8	89	116
$df/d\varepsilon$ (GHz)	0.9	2.06	6.02

the 100 µm-thick sample. To check it, simulations with higher sample thicknesses have been performed and give similar results. For the 100 µm-thick sample, simulations have been performed with several ε_r values and results are shown in Figure 5.

Destructive frequency is shifted because changing ε_r modifies the optical length difference between the two branches. Indeed, the effective refractive index at the sample place becomes $n_s = \sqrt{\frac{\varepsilon_g+\varepsilon_r}{2}}$. The frequency shift as a function of permittivity shift depends on the chosen non-equilibrated structure. Table 1 shows that the interferometer sensitivity increases with the central peak frequency. Considering small variations of $\varepsilon_r = 1+d\varepsilon$, the destructive interference frequency is $f = f_0 + df$. f_0 is the destructive frequency of the non-equilibrated structure previously described, and corresponds to the geometrical path length difference $\delta_0 = n\Delta L$.

To explain the sensitivity increase, f can be expressed as follows:

$$f = f_0 + df \sim \frac{c}{2\delta_0} - \frac{2{f_0}^2}{c} d\delta \tag{3}$$

with $d\delta$ the optical length difference caused by the first-branch sample:

$$d\delta = l \cdot \left(\sqrt{\frac{\varepsilon_q + 1}{2}} - \sqrt{\frac{\varepsilon_q + \varepsilon_r}{2}} \right) \tag{4}$$

Combining these equations leads to the expression of the frequency shift df:

$$df = \frac{4{f_0}^3}{c^2} \cdot l \cdot \Delta L \cdot \frac{d\varepsilon}{4} \tag{5}$$

Since ΔL is proportional to f_0^{-1}, the interferometer sensitivity is proportional to f_0^2, which explains the increase observed in Table 1. It has to be noted that destructive-frequency measurement-precision decreases with frequency. However, this decrease seems to be linear with f_0, whereas the theoretical sensitivity increase is proportional to f_0^2. It will be seen below that the Goubau interferometer here described enables this central frequency increase up to several THz and thus gives ways to reach higher sensitivities.

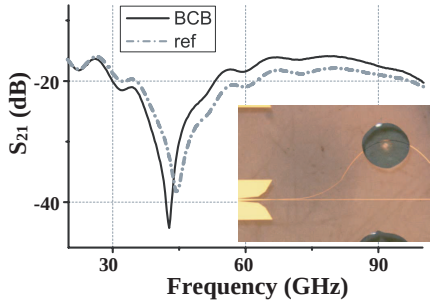

Figure 6. Interferometer transmission as a function of frequency with and without BCB on a branch. Micrograph of the experimental configuration. The destructive frequency for BCB is decreased because the BCB droplet has been put on the longest interferometer branch.

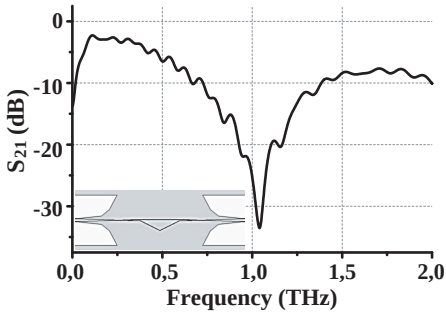

Figure 7. Interferometer structure for 1-THz destructive frequency. Results from CST Microwave Studio simulations.

Experimentally, Cyclotene BCB 3022-46 (thermo sensitive polymer from Dow Chemical [20]) droplets have been manually deposited on one of the interferomter arms and a resonance frequency shift has been observed (Figure 6). By using the Equation (3), the BCB dielectric permittivity has been found equal to 2.8 ± 0.3 in the 40 GHz–110 GHz frequency band. This result agrees with data from Dow Chemical Company ($\varepsilon_r = 2.65$ up to 20 GHz). Measurement uncertainties are mainly due to the droplet shape. Indeed, the droplet height is not constant on the wave path and, at the beginnig and the end of the droplet, the wave is propagated in both air and BCB. To improve measurements accuracy, BCB can be patterned by spin-coating and UV-exposition technological steps in order to obtain a constant heigth BCB sample. Nevertheless, this experiment proves that the interferometer enables to characterize dielectric constants of polymers in the sub-THz frequency band.

4. PERSPECTIVES AND CONCLUSION

It has been previously seen that increasing frequencies is a way to increase the interferometer sensitivity. Moreover, accessing frequencies of the 1–3 THz range is convenient for protein conformation or hydration studies [5]. Here a simulation of the non-equilibrated interferometer structure dedicated to this range is presented. Dimensions of the structure have been chosen by using Equation (2). To avoid perturbative substrate modes, the substrate thickness has been chosen equal to 50 µm in this case. Figure 7 demonstrates that the interferometer topology presented in this communication is well suited for investigations in the whole THz frequency band.

Moreover, to increase measurements sensitivity, multiple reflections coming from THz divider and coupler have to be avoided. Indeed, they decrease the destructive frequency peak resolution. For instance, a resistor can be inserted in the divider/coupler geometry as in the Wilkinson divider topology to the presented structure [21].

The described interferometer is also able to characterize samples in the sub-THz and THz frequency bands. Here, it has been used to probe a droplet-deposited polymer. It has been shown that the interferometer structure enables to obtain, with one measurement step, the same propagation constant usually given by Bianco Parodi two-step measurements. Next work will be the integration of such a structure in microfluidic systems in order to increase sensitivity of differential measurements on biological materials. The interferometer behaviour with highly absorbing materials needs to be tested. Indeed, like resonators, it can be expected that resonance quality will decrease for absorbing samples like water. However, in the interferometric structure, this should be avoided if the losses on the two branches are close. Therefore, it should be possible to compensate the sample high absorption by performing differential measurements with absorbing samples on the two branches.

ACKNOWLEDGMENT

The authors would like to thank Sylvie Lepilliet for high frequency measurements.

REFERENCES

1. Tonouchi, M., "Cutting-edge terahertz technology," *Nature Photonics*, Vol. 1, No. 2, 97–105, 2007.

2. Siegel, P. H., "Terahertz technology in biology and medicine," *IEEE Transactions on Microwave Theory and Techniques*, Vol. 52, No. 10, 2438–2447, 2004.
3. Heh, D. Y. and E. L. Tan, "Modeling the interaction of terahertz pulse with healthy skin and basal cell carcinoma using the unconditionally stable fundamental ADI-FDTD method," *Progress In Electromagnetics Research B*, Vol. 37, 365–386, 2012.
4. Markelz, A. G., "Terahertz dielectric sensitivity to biomolecular structure and function," *IEEE Journal of Selected Topics in Quantum Electronics*, Vol. 14, No. 1, 180–190, 2008.
5. Born, B. and M. Havenith, "Terahertz dance of proteins and sugars with water," *Journal of Infrared Millimeter and Terahertz Waves*, Vol. 30, No. 12, 1245–1254, Dec. 2009.
6. Matvejev, V., C. De Tandt, W. Ranson, J. Stiens, R. Vounckx, and D. Mangelings, "Integrated waveguide structure for highly sensitive thz spectroscopy of nano-liter liquids in capillary tubes," *Progress In Electromagnetics Research*, Vol. 121, 89–101, 2011.
7. Wang, K. L. and D. M. Mittleman, "Metal wires for terahertz wave guiding," *Nature*, Vol. 432, No. 7015, 376–379, 2004.
8. Treizebre, A. and B. Bocquet, "Nanometric metal wire as a guide for THz investigation of living cells," *International Journal of Nanotechnology*, Vol. 5, No. 6–8, 784–795, 2008.
9. Laurette, S., A. Treizebre, and B. Bocquet, "Co-integrated microfluidic and THz functions for biochip devices," *Journal of Micromechanics and Microengineering*, Vol. 21, No. 6, 065029, 2011.
10. Abbas, A., A. Treizebre, P. Supiot, N. E. Bourzgui, D. Guillochon, D. Vercaigne-Marko, and B. Bocquet, "Cold plasma functionalized terahertz biomems for enzyme reaction analysis," *Biosensors & Bioelectronics*, Vol. 25, No. 1, 154–160, 2009.
11. Laurette, S., A. Treizebre, F. Affouard, and B. Bocquet, "Subterahertz characterization of ethanol hydration layers by microfluidic system," *Applied Physics Letters*, Vol. 97, No. 11, 111904, 2010.
12. Treizebre, A., B. Bocquet, Y. S. Xu, and R. G. Bosisio, "New THz excitation of planar Goubau line," *Microwave and Optical Technology Letters*, Vol. 50, No. 11, 2998–3001, 2008.
13. Treizebre, A., M. Hofman, and B. Bocquet, "Terahertz spiral planar Goubau line rejectors for biological characterization," *Progress In Electromagnetics Research M*, Vol. 14, 163–176, 2010.
14. Xu, Y., C. Nerguizian, and R. G. Bosisio, "Wideband planar

Goubau line integrated circuit components at millimetre waves," *IET Microwaves Antennas & Propagation*, Vol. 5, No. 8, 882–885, 2011.

15. Treizebre, A., S. Laurette, Y. Xu, R. G. Bosisio, and B. Bocquet, "THz power divider circuits on planar Goubau lines (PGLS)," *Progress In Electromagnetics Research C*, Vol. 26, 219–228, 2012.
16. Dazhang, L., J. Cunningham, M. B. Byrne, S. Khanna, C. D. Wood, A. D. Burnett, S. M. Ershad, E. H. Linfield, and A. G. Davies. "On-chip terahertz Goubau-line waveguides with integrated photoconductive emitters and mode-discriminating detectors," *Applied Physics Letters*, Vol. 95, No. 9, 092903, 2009.
17. Sepulveda, B., J. S. del Rio, M. Moreno, F. J. Blanco, K. Mayora, C. Dominguez, and L. M. Lechuga, "Optical biosensor microsystems based on the integration of highly sensitive mach-zehnder interferometer devices," *Journal of Optics A: Pure and Applied Optics*, Vol. 8, No. 7, S561–S566, 2006.
18. Lapsley, M. I., I. K. Chiang, Y. B. Zheng, X. Y. Ding, X. L. Mao, and T. J. Huang, "A single-layer, planar, optofluidic Mach-Zehnder interferometer for label-free detection," *Lab on A Chip*, Vol. 11, No. 10, 1795–1800, 2011.
19. Akalin, T. and A. Treizebre, "Microscopy with terahertz biomems," *Proc. of SPIE*, 6186:61860E, 2006.
20. CYCLOTENE Advanced Electronic Resins, *Processing Procedures for CYCLOTENE 3000 Series Dry Etch Resins*, DOW, 2005.
21. Wilkinson, E. J., "An n-way hybrid power divider," *IEEE Transactions on Microwave Theory and Techniques*, Vol. 8, 116–118, 1960.